PROCEEDINGS of the
23rd International Congress on Acoustics

9 to 13 September 2019 in Aachen, Germany

Development of aerial ultrasonic source with cylindrical radiation surface for ultrasonic agglutination

Takuya ASAMI[1]; Hikaru MIURA[2]

[1, 2] Nihon University, Japan

ABSTRACT

We develop a high-power aerial ultrasonic source with cylindrical radiation surface for ultrasonic agglutination. The developed ultrasonic source consists of a bolt-clamped Langevin-type longitudinal vibration transducer, an exponential horn, a resonance rod, and a cylinder-type vibrating plate. Both ends of the cylinder have flanges that do not vibrate. The aerial ultrasonic source resonates at around 28 kHz. The features of the developed ultrasonic source can be applied to ultrasonic agglutination by preventing air leakage through direct connection a pipe and can obtain high sound pressures in the space within the cylinder-type vibrating plate. We describe a design method for the cylinder-type vibrating plate and the vibration characteristics of the developed ultrasonic source. In the proposed design, dimensions for non-vibrating flanges and dimensions for which the cylinder part vibrates and generates high sound pressures were obtained using the COMSOL finite element method. Vibration characteristics show that the designed flanges experience almost no vibration. The obtained sound pressure is around 7 kPa (171 dB) at an input electrical power of around 7 W within the cylinder-type vibrating plate.

Keywords: Ultrasound, Cylindrical, Agglutination, Powder transport, Transverse vibration

1. INTRODUCTION

Applications of high-power aerial ultrasonic waves include agglutination of aerosols and fine particles. It has been recently reported that the power required for powder transport is reduced by irradiating ultrasonic waves during transport (1-4). In such applications, when ultrasonic waves are irradiated by a sound source using a vibrating plate, it is necessary to ensure that structures do not leak the agglutinated mass (5-7).

For such applications, we developed an aerial ultrasonic source using a novel vibrating plate that integrates a conventional vibrating plate and a rigid wall as an aerial ultrasonic source (8, 9). For this novel form, we developed an aerial ultrasonic sound source using a cylindrical vibrating plate with a rigid wall integral structure. This vibrating plate uses a mode in which the node and antinode of transverse vibrations are alternately generated in the longitudinal direction of the cylinder, and the node or antinode of transverse vibration is circularly generated on the circumference perpendicular to the longitudinal direction. Vibration of the rigid wall is very small considering the size of vibrations in the cylindrical part. The obtained sound field is maximized along the central axis within the cylindrical vibrating plate. Such a cylindrical vibration plate can be directly connected to a transport pipe for air containing aerosol, fine particles, etc., by using a rigid wall.

In this paper, we first describe use of the finite element method (FEM) to design a cylindrical vibrating plate with a rigid wall satisfying the above requirements. Next, we clarify basic characteristics of an aerial ultrasonic source using the designed cylindrical vibrating plate with a rigid wall (10).

2. DESIGN OF VIBRATING PLATE WITH RIGID WALL USING FEM

We designed a cylindrical vibrating plate with an integral rigid wall structure using COMSOL Multiphysics 4.4. Specifically, we used FEM for a cylinder (material: A2017 duralumin) with 80-mm inner diameter and 100-mm length. The design was based on a policy by which the vibrational mode of

[1] asami.takuya@nihon-u.ac.jp
[2] miura.hikaru@nihon-u.ac.jp

the vibrating plate alternately generates the node and antinode of transverse vibration along the length direction of the cylinder, and the node or antinode of transverse vibration is circularly generated on the circumference orthogonal to the length direction. A second design policy was realization of large sound pressure along the central axis of the cylinder, with nearly no vibration in the rigid wall.

Figure 1 shows a schematic diagram for the cylindrical vibrating plate to be designed. The cylindrical vibrating plate consists of a cylinder and two rigid walls. The cylindrical vibrating plate has an inner diameter of 80 mm and a length of 100 mm. The thickness T of the cylindrical vibrating plate, the height H of the rigid wall, and the width W are designed using FEM. The design was carried out in the order of drive frequency for the cylindrical vibrating plate, then thickness T of the cylinder, and finally height H and width W of the rigid wall.

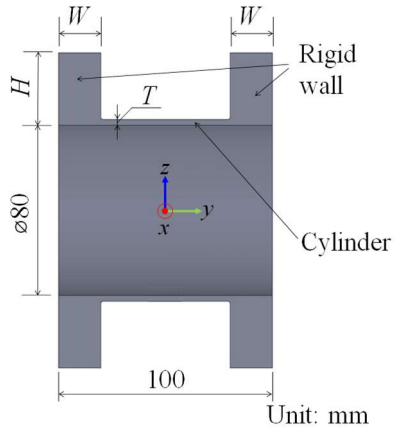

Figure 1 – Cylindrical vibrating plate with two rigid walls

2.1 Determination of Drive Frequency

The driving frequency of the cylindrical vibration plate is determined by focusing on the sound field generated within the cylinder. Concretely, the driving frequency was set to the frequency that maximizes sound pressure of the sound field in the cylinder along the central axis of the cylinder. The node for sound pressure is generated in the radial direction, and the node for concentric circles is generated in the radial direction. We used FEM to calculate the frequency at which the sound field within the cylinder meets the above requirements. Figure 2 shows the model used for analysis. In this analysis, the thickness of the cylinder was adequate, and the entire cylinder was completely fixed. An air layer was installed within the cylinder, and the boundary condition for the air layer at both ends of the cylinder was calculated as 0 Pa pressure.

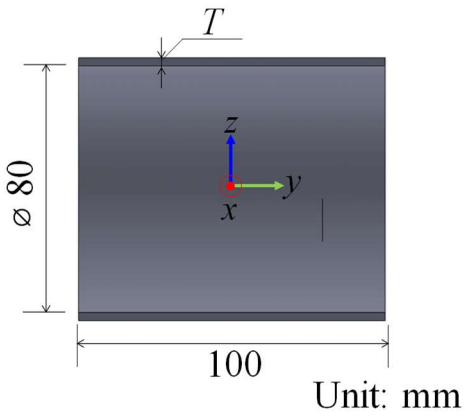

Figure 2 – Reference cylinder for design

Figure 3 shows the frequencies calculated by FEM to obtain the desired sound field mode. Parameters were the number of sound pressure nodes in the radial direction on the horizontal axis, the

frequency at which the desired mode was obtained on the vertical axis, and the number of sound pressure nodes in concentric circles. The figure shows that the frequency increases with the number of nodes in the radial direction at each node in the concentric circle. The results show three desired modes around 28 kHz: at 27.277 kHz (4 radial nodes, 6 concentric nodes), 28.127 kHz (6 radial, 6 concentric), and 27.284 kHz (10 radial, 5 concentric). We therefore consider that the desired sound field mode within the cylinder can be obtained by driving the cylinder at around 28 kHz.

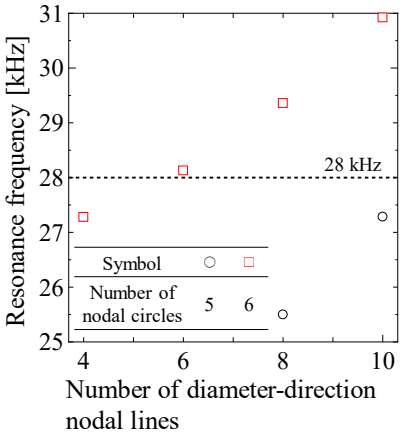

Figure 3 – Relation between number of diameter-direction nodal lines and resonance frequency

2.2 Determination of Thickness *T* of the Cylinder

The thickness *T* of the cylinder is a value by which the node and antinode of transverse vibration are alternately generated in the longitudinal direction of the cylinder in its vibration mode at 28 kHz, and the node or antinode of the transverse vibration is circularly generated on the circumference orthogonal to the longitudinal direction. Thickness *T* is calculated using FEM so that the transverse vibration of the cylinder realizes such a mode. The analytical model is similar to that in Fig. 2. Both ends of the cylinder were perfectly fixed in the analysis, and the frequency at which the desired vibrational mode was obtained was calculated by changing thickness *T*. Unlike the description in Section 2.1, there is no air layer inside the cylinder. The material used for the cylinder is A2017 duralumin, Young's modulus is 76.5 GPa, Poisson's ratio is 0.33, and density is 2,790 kg/m^3.

Figure 4 shows the frequency at which the desired vibrational mode is obtained when thickness *T* as determined by FEM is changed. In Fig. 4, the horizontal axis represents the thickness *T* and the vertical axis represents the frequency at which the desired vibration mode is obtained. The number of circular vibration nodes *n* is taken as a parameter and includes two numbers for the circular nodes generated by completely fixing both ends of the cylinder as per the analysis conditions. As a result, the frequency at which the desired vibrational mode is obtained increases with thickness *T* for each number of circular nodes *n*. This shows that the values for thickness *T* at which the desired vibrational mode is obtained at 28 kHz are 1.4 and 2.7 mm. Considering the working method and strength of the vibration plate, we set thickness *T* for the cylinder to 2.7 mm.

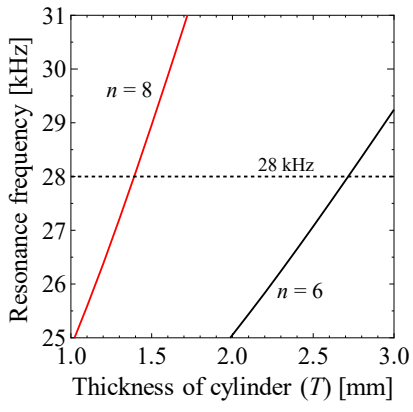

Figure 4 – Relationship between thickness of cylinder (*T*) and resonance frequency

2.3 Determination of Height *H* and Width *W* of Rigid Walls

As Fig. 1 shows, to keep the mode of the sound field within the cylinder unchanged, the rigid wall is integrated with the cylinder and made to protrude inward without changing the length (100 mm). Values for height H and width W of the rigid wall were calculated so that the rigid wall nearly does not vibrate when the cylinder vibrates in the desired mode, and so that the frequency hardly changes from 28 kHz. Figure 1 shows the analytical model. In the analysis, the boundary condition for the overall model was made to be free, and height H and width W of the rigid wall were varied. The frequency and maximum value of vibrational displacement in each part were calculated for the case where the cylindrical part (T = 2.7 mm section) has the desired vibrational mode. Evaluation of the calculation results for frequency was according to the difference between the obtained frequency and 28 kHz. Evaluation of the calculation results for vibrational displacement was according to the ratio between the maximum vibrational displacement of the rigid wall part and that of the cylindrical part. The material of the cylinder was A2017 duralumin, as in Section 2.2, and was calculated using the same material constants.

Figure 5 shows the frequency error rates obtained by FEM when height H and width W of the rigid wall are changed. In that figure, the horizontal axis represents width W of the rigid wall, the vertical axis represents height H of the rigid wall, and the error rate is shown as a contour diagram. The results show that the error rate for the frequency is small in a rigid wall width W range of 19–20 mm, regardless of the height H. We therefore consider that a width of 19–20 mm has little effect on the vibrational mode of the cylindrical part, because it is almost equal to 1/2 the wavelength of transverse vibrations when a cylinder without a rigid wall vibrates in the desired mode.

Figure 6 shows the ratios obtained by dividing the maximum vibrational displacement of the rigid wall by the maximum vibrational displacement of the cylindrical part when height H and width W of the rigid wall are changed. In the figure, the horizontal axis represents width W of the rigid wall and the vertical axis represents its height H. The results show that the ratio of vibration was about 6% between W = 18 mm, H = 40 mm and W = 24 mm, H = 28 mm, which was smaller than other dimensions. In that range, the rigid wall nearly did not vibrate in comparison with the cylindrical part. From the results in Figs. 5 and 6, H = 20 mm and W = 34 mm are the values at which the rigid wall almost does not vibrate when the frequency is near 28 kHz.

In summary, from this FEM-based design, the driving frequency was 28 kHz and the dimensions were T = 2.7 mm, W = 20 mm, and H = 34 mm.

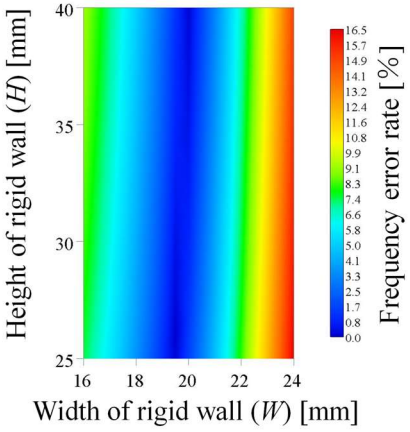

Figure 5 – Relation between dimensions H and W of rigid walls and frequency error rate

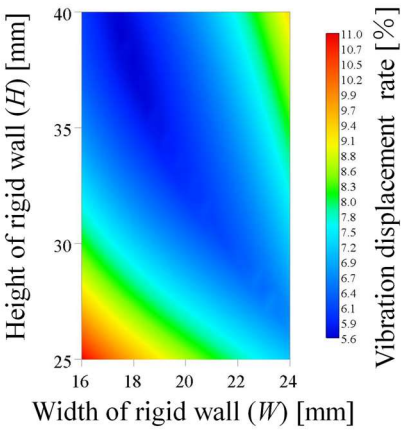

Figure 6 – Relation between dimensions H and W of rigid walls and vibration rate

2.4 Aerial Ultrasonic Source Using Cylindrical Vibrating Plate With Rigid Walls

Figure 7 shows a schematic diagram for an aerial ultrasonic source using a cylindrical vibrating plate with rigid walls using the FEM-designed values. The aerial ultrasonic source consists of a bolt-clamped Langevin ultrasonic transducer for 27 kHz, an exponential horn for expansion of

longitudinal vibration displacement amplitude, a transmission rod, and a cylindrical vibrating plate (material: A2017 duralumin). Each part is connected by a screw.

The rigid wall part of the cylindrical vibrating plate is connected to both ends of the cylindrical part as an integral structure. The cylindrical vibrating plate has a hole with 5-mm diameter in its center for connection with the transmission rod. A concave washer and a convex washer are inserted into the coupling between the vibrating plate and the transmission rod to facilitate propagation of longitudinal vibrations from the transmission rod. The coordinate axis shown in Fig. 1 was set with the cylinder center at the origin for measurements.

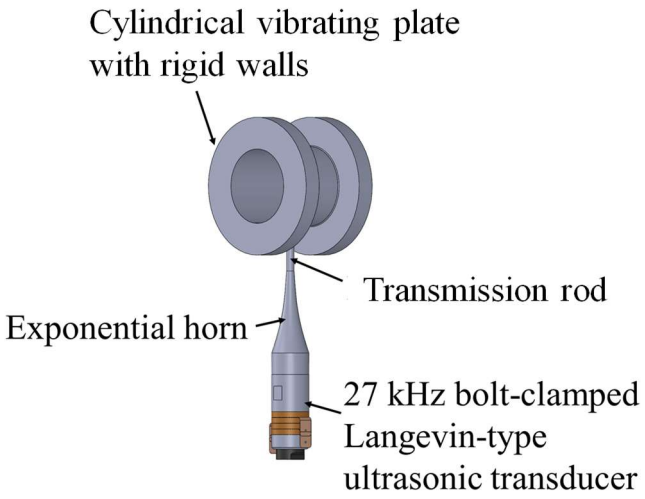

Figure 7 – Aerial ultrasonic source using a cylindrical vibrating plate with rigid walls

3. VIBRATION CHARACTERISTICS OF THE AERIAL ULTRASONIC SOURCE

This chapter experimentally examines whether the desired sound field and vibrational mode are obtained by the FM-designed cylindrical vibrating plate.

3.1 Sound Pressure Characteristics for Frequency at the Cylindrical Vibrating Plate Origin

To clarify whether a large sound pressure is obtained along the central axis of a cylinder generating the desired sound field by a cylindrical vibrating plate, we measured sound pressure characteristics for the frequency at the origin of the cylindrical vibrating plate. We measured the sound pressure using a 1/8-inch condenser microphone (ACO, 7118) with a constant driving voltage of 5 V_{rms} and driving frequency varying from 27.5 to 28.5 kHz.

Figure 8 shows the results, with the horizontal axis representing the driving frequency and the vertical axis representing the sound pressure. The figure shows that the sound pressure had local maximum values at driving frequencies of 27.64, 27.82, and 28.27 kHz. The sound pressure of about 1.8 kPa at 27.64 kHz is particularly large, as compared with other local maximum values. These results suggest that the desired sound field is obtained at 27.64 kHz.

3.2 Sound Pressure Distribution Inside the Cylindrical Vibrating Plate

We next measured the sound pressure distribution inside the cylindrical vibrating plate to clarify whether the desired sound field is obtained at the frequency from section 3.1. We measured the sound pressure distribution in the x–y plane within the cylinder using a 1/4-inch condenser microphone (ACO, 7016) with a probe when the driving frequency was 27.64 kHz and the driving power was 0.1 W.

Figure 9 shows the results. The horizontal axis shows the position on the y-axis, the vertical axis shows the position on the x-axis, and contours show the sound pressure normalized by the maximum value. This figure shows that there are 12 nodal lines parallel to the y-axis direction, because six concentric circular nodes are generated in the radial direction of sound pressure. We also found that the maximum sound pressure occurs on the central axis of the cylindrical vibrating plate, and that there were four sound pressure nodes parallel to the x-axis, that is, in the radial direction of the sound pressure. The obtained sound pressure distribution was almost the same as that obtained in Fig. 3 for

27.277 kHz. These results show that the sound field in the cylindrical vibrating plate was nearly according to design, as was the driving frequency.

We measured sound pressure at the origin while varying the input power, using a 1/8-inch condenser microphone (ACO, 7118) as in Section 3.1. The input power was up to 7 W.

Figure 10 shows the results, with input power on the horizontal axis and sound pressure on the vertical axis. These results show that the sound pressure is approximately proportional to the square root of the input power. The sound pressure was about 8 kPa at an input power of 7 W. The sound pressure exceeds measurement limits of the microphone at higher input powers, so in this study we limited input power to 7 W. However, it previously has been confirmed that an aerial ultrasonic source can be driven to about 50 W. If the sound pressure remains proportional to the square root of the input power, a sound pressure of about 20 kPa can be obtained from an input power of about 50 W.

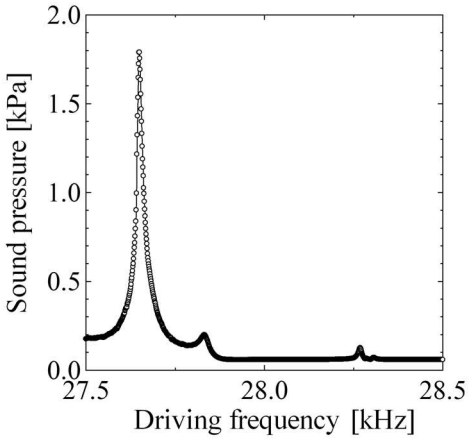

Figure 8 – Relation between driving frequency and sound pressure at the origin

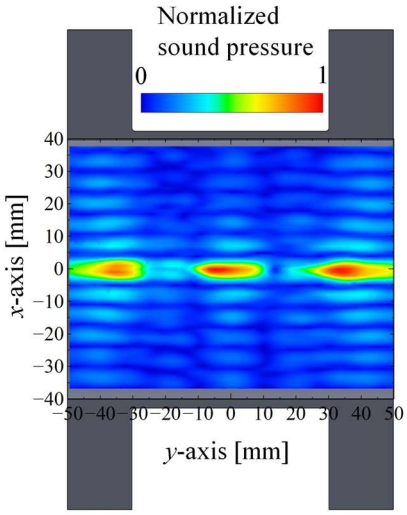

Figure 9 – Sound pressure distribution within the vibrating plate in the x–y plane

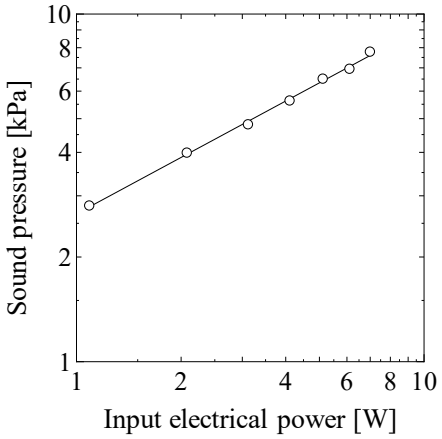

Figure 10 – Relation between input electric power and sound pressure at the origin

3.3 Transverse Vibrational Distribution in the Cylindrical Vibrating Plate

We next measured the distribution of transverse vibration in a cylindrical vibrating plate to clarify whether the node and antinode of transverse vibration are alternately generated in the longitudinal direction (y-axis) of a cylinder with a cylindrical vibrating plate in the desired vibration mode, and whether the node or antinode of transverse vibration is circularly generated on the circumference orthogonal to the longitudinal direction (y-axis). The deflection vibration distribution in the y-axis

direction of the cylindrical vibrating plate outer diameter was obtained using a laser Doppler vibrometer (Ono Sokki, LV -1610) when the driving frequency was 27.64 kHz and the driving electric power was 1 W.

Figure 11 shows the results, with the position in the *y*-axis direction on the horizontal axis, the amplitude of transverse vibration displacement on the vertical axis, and the measurement point indicated in the schematic diagram. This figure shows that transverse vibrational displacement of the cylindrical part (T = 2.7 mm section) had four nodes in almost the same position at all measurement points. This shows that the node of transverse vibrational displacement became four nodes symmetrical about the *y*-axis, which is the central axis, and that the node of transverse vibrational displacement is circular. However, the distribution of transverse vibration, shown by the plotted triangles (△), indicates smaller values for vibrational displacement at measurement points near the transmission rod than that at other points. This is likely because transverse vibration at the cylindrical part was suppressed by longitudinal vibrations of the transmission rod. In the rigid wall, transverse vibrational displacement is at most about 0.1 μm at all measurement points, while transverse vibration in the cylindrical part (*T* = 2.7 mm section) becomes about 2.4 μm at the antinode position and about 0.1 μm in the node position of the vibrational distribution. These results show that transverse vibration of the rigid wall was small and nearly the same value as the nodal position of the cylindrical part, and that the desired design was obtained with four node lines and little vibration of the rigid wall.

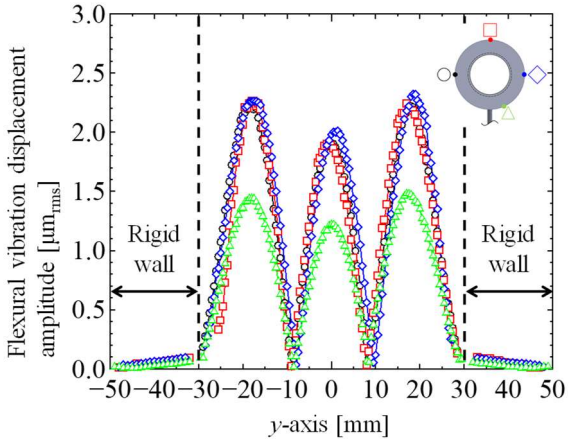

Figure 11 – Transverse vibrational displacement distribution

at the outer diameter of the vibrating plate

4. CONCLUSIONS

We presented an FEM-based design for a cylindrical vibrating plate integrated with rigid walls. We also presented basic characteristics of an aerial ultrasonic source using the designed cylindrical vibrating plate. Design of the cylindrical vibrating plate started with FEM analysis using COMSOL Multiphysics 4.4, from which we decided on a driving frequency and dimensions for the cylindrical vibrating plate focusing on the sound field within the cylinder and the vibrational mode of the cylindrical vibrating plate. We then measured the basic characteristics of an aerial ultrasonic source using the vibrating plate.

As a result, the sound field within the circular vibrating plate attained maximum values along the central axis of the cylindrical vibrating plate. In vibrations in the cylindrical part of the vibrating plate, the node and antinode of transverse vibrations are alternately generated in the length direction of the cylinder, and the node or antinode of transverse vibration is circularly generated on the circumference orthogonal to the length direction. Vibration of the rigid wall part had nearly the same value for displacement amplitude as did the nodal position of transverse vibration of the cylindrical part. This demonstrated that the rigid wall part hardly vibrates, showing that a cylindrical vibrating plate with an integral rigid wall structure can be designed using FEM.

References

1. J. A. Gallego-Juárez, E. R.-F. De Sarabia, G. RodrÍguez-Corral, T. L. Hoffmann, J. C.

Gálvez-Moraleda, J. J. RodrÍguez-Maroto, F. J. Gómez-Moreno, A. Bahillo-Ruiz, and M. M.-E. Acha. Application of Acoustic Agglomeration to Reduce Fine Particle Emissions from Coal Combustion Plants. Environ. Sci. Technol. 33, 3843 (1999).
2. Endo, M. Yanagimoto, T. Asami, and H. Miura. Noncontact atomization of droplets using an aerial ultrasonic source with two vibrating plates. Jpn. J. Appl. Phys. 54, 07HE13 (2015).
3. L. D. Rozenberg, Physical Principles of Ultrasonic Technology (Plenum, New York, 1973) Vol. 2, Part X.
4. K. Kofu. Pressure loss reduction in horizontal plug conveying of granular particles with ultrasonic vibration. Powder Technol. 294, 202 (2016).
5. J.A. Gallego-Juárez, and K. F. Graff, Power Ultrasonic (Elsevier, Amsterdam, 2015) Chap. 7.
6. Y. Ito. High-intensity aerial ultrasonic source with a stripe-mode vibrating plate for improving convergence capability. Acoust. Sci. Technol. 36, 216 (2015).
7. K. Naito, T. Asami, and H. Miura. Formation of aerial standing wave field using ultrasonic sources consisting of multiple stripe-mode transverse vibrating plates. Jpn. J. Appl. Phys. **54**, 07HE07 (2015).
8. R. Sato, T. Asami, and H. Miura. Ultrasound source using a rectangular vibrating plate combined with rigid walls. Jpn. J. Appl. Phys. **56**, 07JE05 (2017).
9. R. Kuratomi, T. Asami, and H. Miura. Aerial ultrasound source with a circular vibrating plate attached to a rigid circumferential wall. Jpn. J. Appl. Phys. **57**, 07LE06 (2018).
10. T. Asami and H. Miura. Development of aerial ultrasonic source using cylinder typed vibrating plate with axial nodal mode. Jpn. J. Appl. Phys. **57**, 07LE11 (2018).